Pergamon

Journal of Structural Geology, Vol. 19, No. 9, pp. 1219 to 1230, 1997

0191-8141/97 $17.00 + 0.00

PII: S0191-8141(97)00037-0

Raft tectonics: the effects of basal slope angle and sedimentation rate on progressive extension

T. MAUDUIT

Géosciences Rennes, UPR 4661 CNRS, Campus de Beaulieu, Rennes 35042, France

G. GUERIN

ELF Norge, Stavanger Norway

J.-P. BRUN

Géosciences Rennes, UPR 4661 CNRS, Campus de Beaulieu, Rennes 35042, France

and

H. LECANU

ELF Aquitaine Production, Avenue larribau, Pau 64018, France

(*Received* 4 *October* 1996; *accepted in revised form* 7 *April* 1997)

Abstract—In the Gulf of Guinea, the Upper Cretaceous–Tertiary sedimentary cover has undergone gravity gliding above an Aptian salt layer for various basal slope angles from 0° to 4°. Gliding started during Albian time and evolved up to the present with variable sedimentation rates. Faulting patterns are seen to vary in particular as a function of the basal slope angle and the syn-kinematic sedimentation rates. A series of laboratory experiments on small-scale models is used to study the effects of the two parameters mentioned above. Models are composed of two-layer slabs, with Newtonian silicone putty at the base to represent a basal salt décollement and dry sand on top to represent the sedimentary overburden. Models are allowed to deform under their own weight for various basal slope angles ranging from 0° to 5° with two different syn-kinematic sedimentation rates. It is shown that the basal slope angle α controls the location of faulting in the overburden, within a single downslope deformation domain for α values smaller than 2° and within two domains lying downslope and upslope for higher values of α. The width of the deformation domains also varies as a function of α. Overburden faulting always starts with syn-kinematic grabens which evolve into symmetric or asymmetric grabens or into tilted blocks bounded by listric normal faults. While synthetic listric normal faults characterize the downslope deformation domains, both synthetic and antithetic listric normal faults can occur in the upslope deformation domain. Ductile deformation within the basal décollement layers results from variable combinations of pure shear and simple shear. Interaction of ductile deformation in the ductile décollement layer with faulting in the overburden locally produces complex and heterogeneous strain patterns, notably within salt rollers. Finally, increasing rates of syn-kinematic sedimentation are seen to increase the rate of downslope displacement and to enhance and favour the development of listric normal faults. © 1997 Elsevier Science Ltd.

INTRODUCTION

The post-rifting sedimentary cover of passive margins can undergo large-scale gravity gliding even when the basal slope is extremely shallow dipping (less than 1°), if an efficient layer of décollement (e.g. salt) is present at the base. Gliding-induced deformation produces a large variety of growth faulting structures, which are extensional upslope (i.e. landward) and compressional downslope (i.e. seaward). Oil industry exploration has provided spectacular seismic images of these structures, especially for the Atlantic margins of Africa (Jackson and Cramez, 1989; Duval *et al.*, 1992; Lundin, 1992; Liro and Coen, 1995; Spathopoulos, 1996) and Brazil (Cobbold and Szatmari, 1991; Demercian *et al.*, 1993; Mohriak *et al.*, 1995; Szatmari *et al.*, 1996). Laboratory experiments on small-scale models greatly improve the understanding of the processes of faulting and of interactions between faulting and synchroneous sedimentation (Vendeville, 1987; Vendeville and Cobbold, 1988; Cobbold and Szatmari, 1991; Vendeville and Jackson, 1992a,b; Gaullier *et al.*, 1993).

In the present paper, we first present some characteristic structures induced by gravity gliding in the Gulf of Guinea and, second, a series of laboratory experiments to analyse the effects of the basal slope angle and deformation rates on the development of gliding-induced extensional structures on passive margins. From the experimental results, and through a comparison with natural examples, we discuss some simple rules for progressive deformation and structure development within syn-sedimentary glided slabs.

GRAVITY-DRIVEN DEFORMATION IN THE GULF OF GUINEA

The structural history of the Gulf of Guinea starts with a rifting event during the Early Cretaceous, followed by the deposition of a post-rift marine sequence with an Aptian salt layer at its base. The post-rift sequence is affected by gravitational gliding above the Aptian evaporites, which act as a regional-scale décollement. Structures attesting for gravitational gliding are diachronous in space from Angola to the south to the Niger Delta to the north. For details the reader can refer to previous regional studies by Burollet (1975), Jackson and Cramez (1989), Teisserenc and Villemin (1990), Duval *et al.* (1992), Lundin (1992), Liro and Coen (1995) and Spathopoulos (1996).

A selection of three seismic sections are presented from the Gulf of Guinea (see location on Fig. 1) to illustrate characteristic structures resulting from gravitational gliding as a function of the initial basal slope angle (Figs 2 & 3) and of the sedimentation rate (Fig. 4).

The geological section of the Congo margin, presented in Fig. 2, outlines the effects of a low initial basal slope angle (α) on deformation partitioning in the overburden. Note that, despite the vertical exageration, the base of the slided units remains extremely shallow dipping. The SW–NE regional section drawn on the basis of original seismic lines (Fig. 2a) displays a deformed zone located downslope while the 60 km landward section remains undeformed. Well data indicate that the present-day thickness of the salt layer is around 500 m. Further northeast, the salt basin is bounded by outcrops of pre-Aptian basement. The basal slope calculated from well data is less than 1°. Southwest of the section, two normal listric faults with associated roll-over anticlines (1 and 2 on Fig. 2b) were active during Albian times and are capped by mid-Cenomanian sediments. A detailed analysis of layer geometry in the hanging-wall wedges shows that fault 1 initiated first and has constantly accommodated more displacement than fault 2.

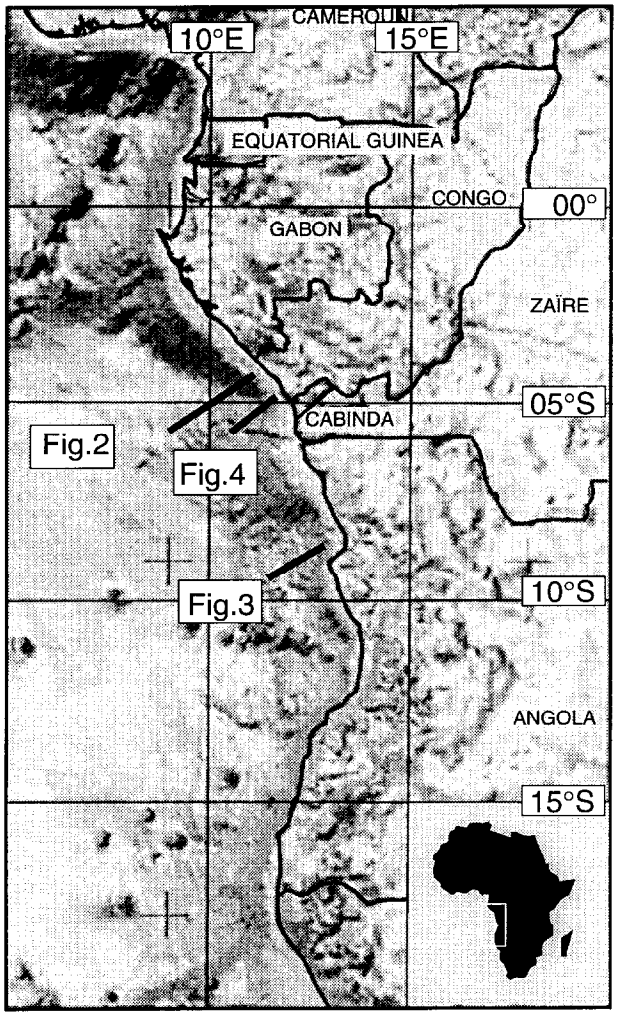

Fig. 1. Location of sections presented in Figs 2–4 (Gulf of Guinea).

The geological section of the Angola margin shown in Fig. 3 illustrates the effects of a higher initial basal slope on deformation partitioning in the Albian cover. Over a distance of 80 km within Albian formations, it displays numerous small tilted blocks controlled by normal faults dipping dominantly to the southwest. The basement crops out 15 km to the northeast of the faulted zone outside the section. Although no well data were available in the area, a dip angle of 4° is estimated using depth conversion for the envelope of Aptian basement. The estimated dip for the Upper Cretaceous formation which correspond to the top of the deformed section is less than 1° (Fig. 3a). This indicates that the 4° slope existed during the thin-skin extension.

The seismic section from the Congo margin (Fig. 4) shows the possible effects of an increase in sedimentation rate. In south Congo, the thin-skinned extension took place mainly from Albian to Cenomanian. Translation and associated extension remain moderate during the Lower–Middle Albian, and increased during the Upper Albian–Lower Cenomanian, leading to significant rafting. Figure 4 shows a large Upper Albian–Lower Cenomanian growth structure separating Lower–Middle Albian rafts. The present-day slope of the basal décollement is around 3–4° toward the southwest, mainly due to a Tertiary regional tilting event during the Tertiary. Indeed, well data indicate that the thickness of the deformed overburden (i.e. from Aptian salt to top Cenomanian) is nearly constant along the section (around 1750 m). This suggests that the overburden has been rafted over a low dipping basal slope (less than 0.5°) and that the rapid increase in translation during the Upper Albian was not related to any variation of the slope angle. On the other hand, the well data also indicate that during the Upper Albian–Lower Cenomanian the sedimentation rate is three times higher than during the Lower–Middle Albian. It is therefore proposed that the translation of 15 km of the downslope raft (Fig. 4) and, more generally, the increase in extension during the Upper Albian–Lower Cenomanian times are directly related to an increase in the sedimentary supply.

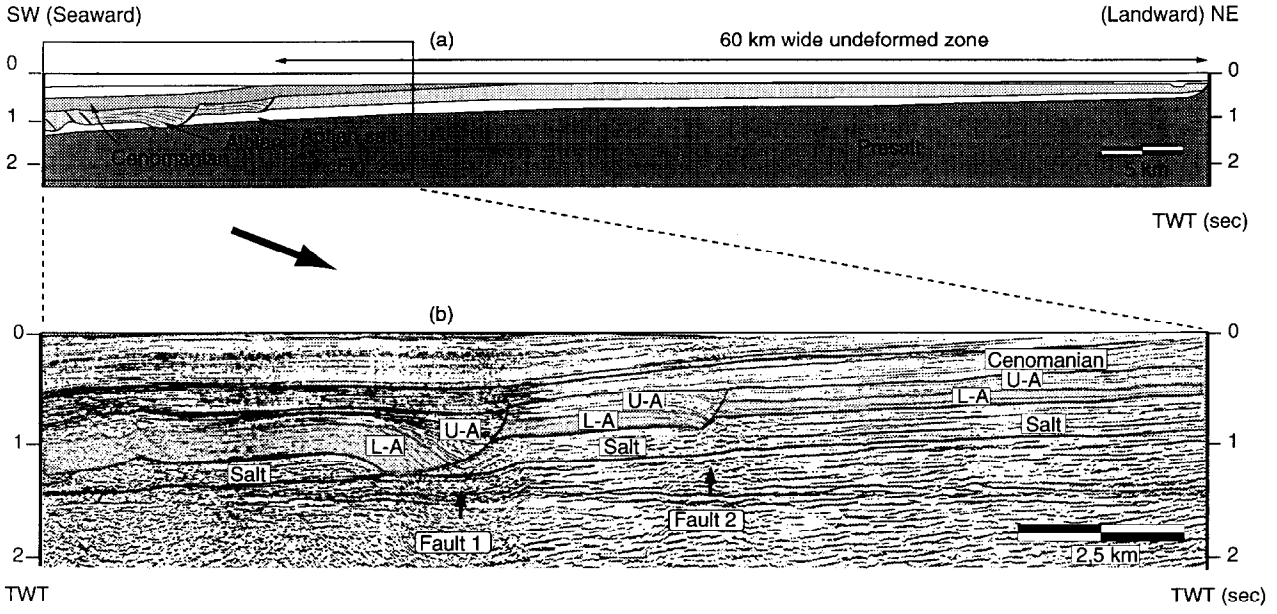

Fig. 2. Section displaying the effect of basal slope on deformation partitioning with a low slope angle (see location on Fig. 1). (a) Regional-scale section showing a 60-km wide undeformed zone and a downslope deformed zone. (b) Enlargement of the deformed zone showing two normal listric faults with associated roll-over anticlines (1 and 2) active during the Albian and capped by mid-Cenomanian sediments. Layer geometry in the hanging-wall sedimentary wedges shows that fault 1 initiates first and permanently accommodates more displacement than fault 2. LA, Lower Albian; UA, Upper Albian.

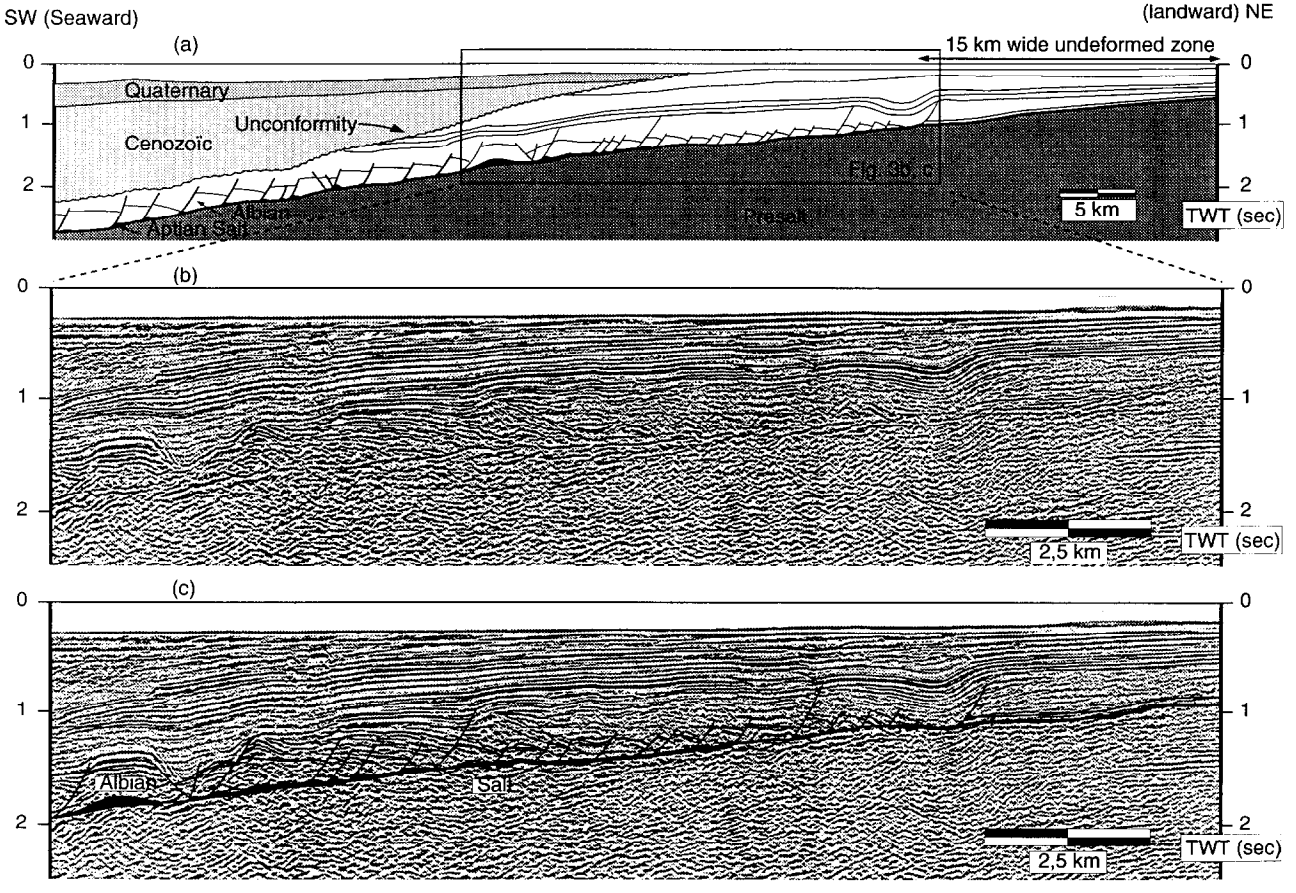

Fig. 3. Section displaying the effect of basal slope on deformation partitioning with a high slope angle (see location on Fig. 1). (a) Regional-scale section showing deformation distributed over a wide area with short fault spacing. Faults are capped during Upper Cretaceous times. (b) & (c) Enlargement of the upslope part of the deformed area.

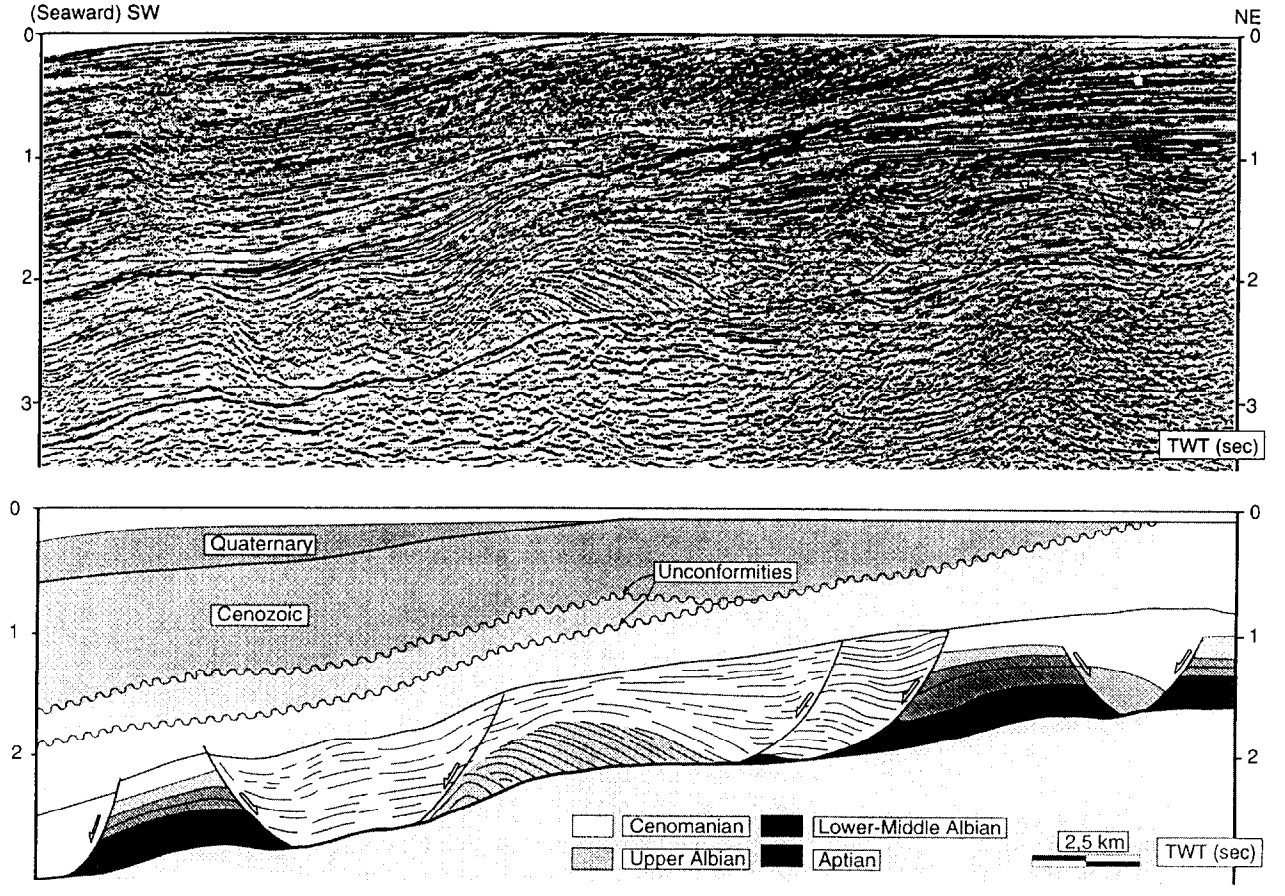

Fig. 4. Section displaying the effect of variations in sedimentation rate. During rafting, the slope of the pre-Aptian basement top was lower than 1°. The total displacement recorded by the large growth structure (located in the middle part of the section) is around 15 km and was acquired during the Upper Albian–Lower Cenomanian without any variation of the basal slope.

The three examples given above illustrate the possible role of the basal slope angle and the sedimentation rate on syn-sedimentary deformation during gravity gliding. If the slope angle is low, deformation is localized at a few fault sites at the seaward edge of the margin (Fig. 2). If the slope angle is higher, the number of faults increases indicating distributed deformation and displacement (Fig. 3). In these two examples, the sediment supply during gliding is low. However, at places where sedimentation supply during gliding is high, displacement rate is seen to increase with time (Fig. 4). These lines of evidence led us to explore the potential interactions between sedimentation and deformation during gravity gliding through laboratory experiments on small-scale models.

ANALOGUE MODELLING

Previous work

Since the pioneering work of Cloos (1968), various types of experimental study on gravitational gliding have been attempted. In all of them it is generally assumed that the direction of displacement depends on the dip of the décollement surface and/or the basal slope (Crans *et al.*, 1980). On passive margins, both of these slopes dip towards the ocean basin. In recent years, scaled physical models have been used to study various aspects of gravitational gliding upon a salt layer (Vendeville, 1987; Vendeville *et al.*, 1987; Vendeville and Cobbold, 1988; Vendeville and Jackson, 1992a,b; Gaullier *et al.*, 1993). At early stages of gliding, these models generally exhibit three structural domains: an undeformed central block undergoing translation, which separates two domains of normal faulting. During synchronous deformation and sedimentation, block tilting is accommodated by growth faults which more generally dip downslope.

Modelling material and scaling

The scaled physical models presented in the following sections were performed in the Laboratory of Experimental Tectonics at Géosciences Rennes. All the experiments are scaled-down replicas of natural examples with simplified rheological and mechanical properties. Rock salt is assumed to be a Newtonian viscous fluid with a viscosity ranging from 10^{16} to 10^{18} Pa s^{-1} and a mean density of 2200 kg m^{-1}. Salt is modelled using silicone

putty manufactured according to the specification GS1^R by Rhone Poulenc (France), with densities ranging between 1400 and 1550 kg m^{-3} and viscosities between 1.15×10^4 and 1.50×10^4 Pa s^{-1} at 30°C (see Nalpas and Brun, 1993, appendix 1). Changes in salt viscosity due to changes in strain rate, temperature or water content are small and can be disregarded. Sedimentary rocks and basement are assumed to be brittle and to deform according to a Mohr–Coulomb criterion of failure with negligible cohesion and a mean angle of internal friction of 30° (Hubbert, 1937, 1951; Byerlee, 1968). Experiments do not account for potential effects of fluid pressure and sediment compaction. A well-sorted fine-grained (500 μm) dry quartz sand with a density of about 1300 kg m^{-3} is used to represents both sedimentary overburden and basement rocks.

Experiments are designed to respect conditions of dynamic similarity between the model and the natural example as defined by Hubbert (1937), Ramberg (1967) and Davy (1986).

Apparatus and experimental procedure

Models were built in a 43 × 100 cm box (Fig. 5), and consist of a 1-cm thick silicone layer to represent the Aptian salt overlain by a sand overburden to represent Albian–Cenomanian sedimentary rocks. The brittle overburden is composed of a 1–2-cm thick 'pre-kinematic' layer which corresponds to Lower Albian sediments deposited over the basal silicone layer before the onset of extension. The box is then inclined with a variable basal slope angle α, kept constant during a given experiment and the downslope endwall of the box is removed to allow free gliding. Deposition of syn-kinematic layers representing Upper Albian–Upper Cretaceous sediments is simulated by means of the sequential deposition of 0.4-cm thick sand layers with contrasting colours but identical isotropic mechanical properties. However, the thickness of the 'syn-kinematic' elementary layers is never unifom due to structural irregularities associated with block faulting and tilting. Top views were taken at regular time intervals, before and after deposition of each new layer.

After the experiment, models were overlain by a 'post-kinematic' cover to preserve final topography, to facilitate cutting and to prevent further model deformation. Models were then sprayed with water to make the sand more cohesive, allowing parallel sections at 5-cm intervals. To escape structural perturbations due to lateral boundary shear, only sections from the centre of models are shown here.

The basal silicone layer was built with bands of two alternating colours (Figs 5–7) to obtain vertical passive markers whose later deformation helps reveal the finite strain resulting from gravity gliding within the ductile layer.

During the project, 19 experiments were performed to study the effects of basal slope and sedimentation on gravitational gliding (see Table 1). Only a selection of these experiments are presented and discussed here. In the two first sets, the thickness of the pre-kinematic overburden is fixed at 1 or 2 cm, the basal slope angle ranges from 0° to 5° in steps of 1° and the syn-kinematic sedimentation rate is low (0.2 cm h^{-1}). In the two following sets (3 and 4, Table 1) the sedimentation rate is high (0.4 cm h^{-1}). For these two latter sets, only a few values of the α angle between 0° and 5° are tested.

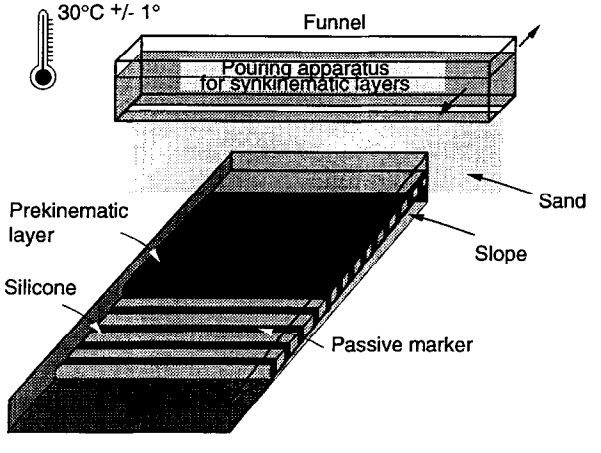

Fig. 5. Experimental apparatus used to model the sedimentary cover gliding above a salt layer on a passive margin. The model is composed of a lower viscous layer (silicone) representing Aptian salt and an upper brittle overburden (sand). A mobile funnel is used to pour regular syn-kinematic layers of constant thickness which represent Upper Albian–Upper Cretaceous sediments. The basal silicone layer is built up with bands of two alternating colours to obtain vertical passive strain markers. The box containing the model is inclined at a basal slope angle α that is kept constant during the experiment.

Deformation domains

Strain patterns within ductile spreading–gliding slabs, such as those considered here, have been described in detail by Brun and Merle (1985, 1988) and Merle (1986). Even if the interaction between brittle and ductile layers in the present experiments leads to more complex structural patterns, the same general trends hold, as observed in previous studies. Deformation in any part of the slab results from a combination of pure shear (i.e. shortening perpendicular to the base) and simple shear (i.e. shearing parallel to the base). The pure-shear component dominates in the upslope part of the slab, but is also present at its downslope end. In the middle part of the slab, flow in the ductile layer approached simple shear. In all experiments, the strain intensity increases downslope. The intensity of mean strain rate in the ductile layer, measured in the central part of the model, increases as a direct function of both basal slope angle and slab thickness.

Figure 6 illustrates the pattern of deformation which occurs in the downslope deformation zone in models with low basal slope angles (0–2°). As previously described by Vendeville (1987) and Gaullier *et al.* (1993), deformation

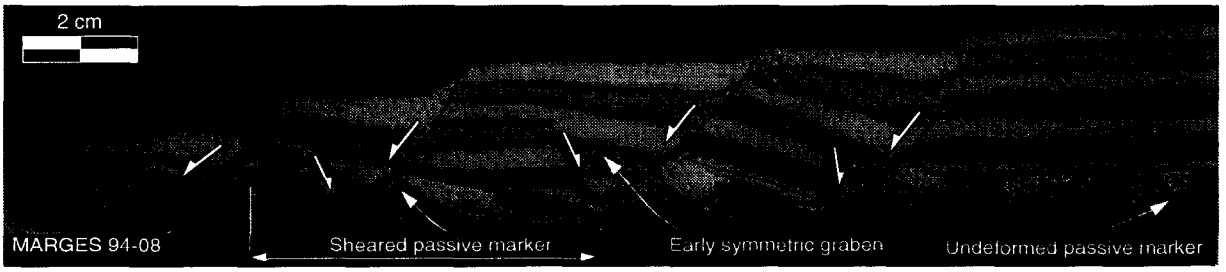

Fig. 6. Typical section of a downslope deformation zone in models with low basal slope angles (0–2°). The dotted line indicates the top of the pre-kinematic layer and the plain line the top of the ductile layer. Deformation within the brittle layer starts with nearly symmetric grabens. During progressive deformation, synthetic normal faults become progressively listric and antithetic normal faults are capped by syn-kinematic sedimentation. Variations in the thickness of initially vertical marker bands result from variations in finite-strain intensity. To the rear of the deformed zone the vertical markers are almost undeformed.

in the brittle layer starts with nearly symmetric grabens. With increasing stretching, antithetic normal faults are draped over by syn-kinematic sedimentation. Draping occurs at very early stages for low α, being subsequently delayed as α increases. Observations of deformation at the surface during experiments reveal that faulting in the downslope deformation domain propagates upward. Towards the rear of the deformed zone, the vertical markers are only slightly deformed showing a downward extrusion of the ductile material. Below the tilted blocks, the initially vertical markers are sheared top to the front. Variations in the thickness of marker bands result from variations in finite-strain intensity. In the vicinity of listric normal faults within the so-called 'salt rollers' (Bally *et al.*, 1981)—in natural equivalent structures—the markers display thickness variation and folding.

Figure 7 shows the three domains of deformation which occur in models with a basal slope angle higher than 2°. Owing to a high basal slope angle (4°) the total displacement is larger than in the model shown in Fig. 6, thus leading to a mean high shear-strain component in the basal ductile layer (mean $\gamma = 12.5$). The following three distinct subpatterns can be distinguished from front to back.

(1) The downslope deformation domain (Fig. 7a) as in Fig. 6, is characterized by a series of tilted blocks below which the ductile layer progressively acquires a jigsaw profile with asymmetric teeth. The geometrical patterns of deformed markers are relatively constant within each tooth of the ductile layer (i.e. under each tilted block). The markers are strongly sheared and thinned, and rotated while remaining nearly parallel to the base of the ductile layer and the brittle–ductile interface. Although the bulk geometrical pattern is similar to the one observed in Fig. 6, it here displays a higher finite-strain intensity.

(2) The central zone (Fig. 7b) is characterized by a

Table 1. Model parameters for the experiments

MARGES experiment No.	Slope (°)	Thickness of the pre-kinematic overburden (cm)	Final length of model (cm)	Bulk stretching (%)	Sedimentation rate*	Refer to:
94-05	0	1	62.0	17.5	LSR	Fig. 11
94-13	1	1	67.0	20.5		Fig. 11
94-14	2	1	65.5	21.0		Fig. 11
94-15	3	1	78.0	50.5		
94-16	4	1	78.0	53.0		
94-08	0	2	59.5	13.0		
94-07	1	2	63.0	20.0		Figs 6–9
94-09	2	2	70.5	19.0		Figs 9–12
94-10	3	2	70.5	17.5		Figs 9–12
94-11	4	2	74.5	30.0		Figs 9–12
94-12	5	2	75.0	32.0		Figs 7, 9–12
94-17	0	1	66.0	15.0	HSR	Fig. 11
94-18	1	1	66.0	19.0		Fig. 11
94-19	2	1	67.5	23.0		Fig. 11
94-20	3	1	66.0	24.0		
94-21	0	2	63.0	15.5		
94-22	1	2	63.0	16.5		
94-23	2	2	70.5	34.5		
94-24	3	2	70.5	34.5		

*LSR, low sedimentation rate; HSR, high sedimentation rate.

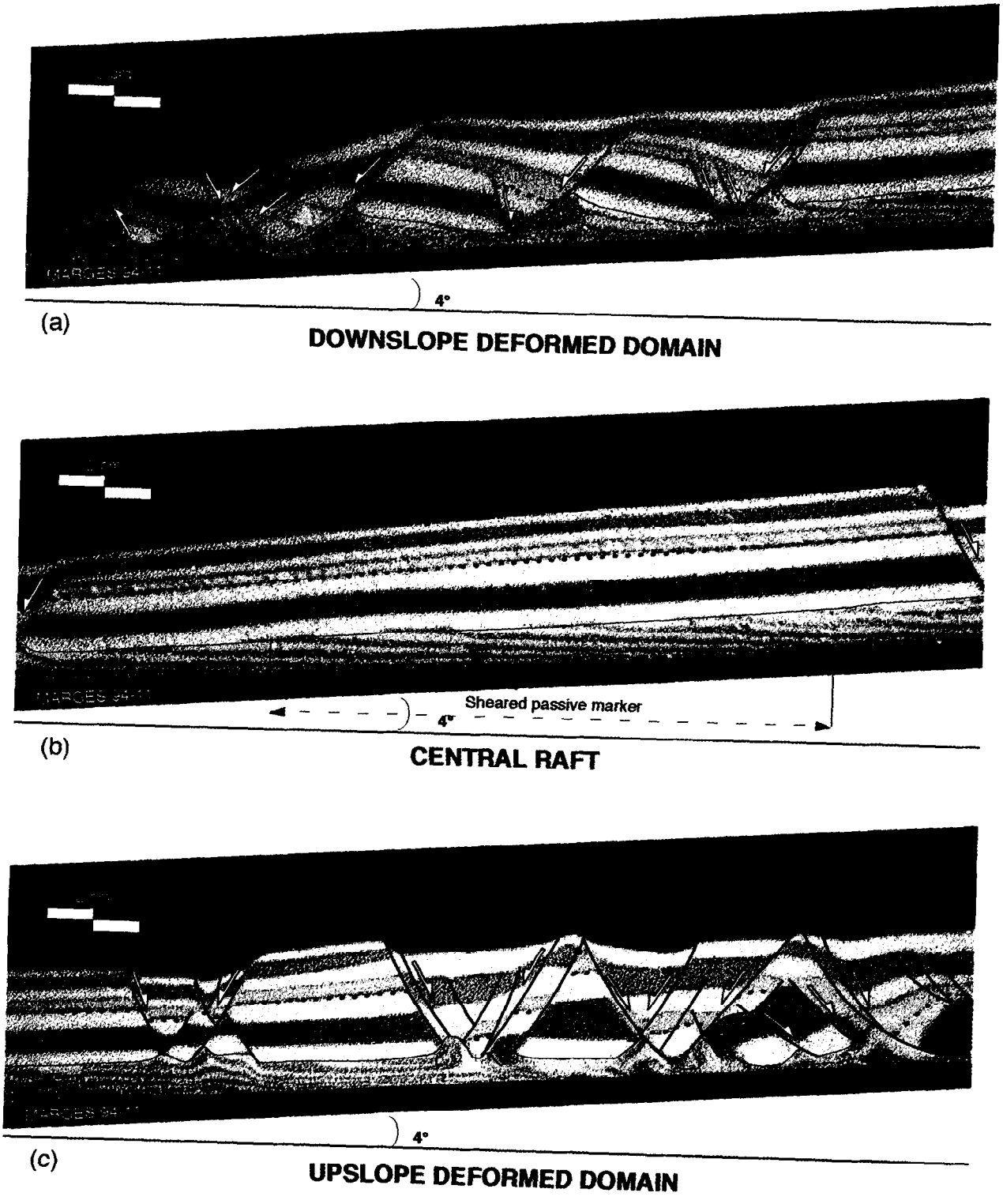

Fig. 7. Domains of deformation in models with basal slope angles higher than 2°. The total displacement is more than in Fig. 6, leading to a higher mean shear-strain component in the basal ductile layer. (a) The downslope deformation domain is characterized by a series of tilted blocks. (b) The central zone is characterized by a large undeformed raft below which the ductile layer is homogeneously and strongly sheared. (c) The upper brittle layer is translated without deformation. The upslope deformation domain is characterized by systems of conjugate planar normal faults, even synthetic or antithetic listric normal faults, which delimit thick syn-kinematic depocentres.

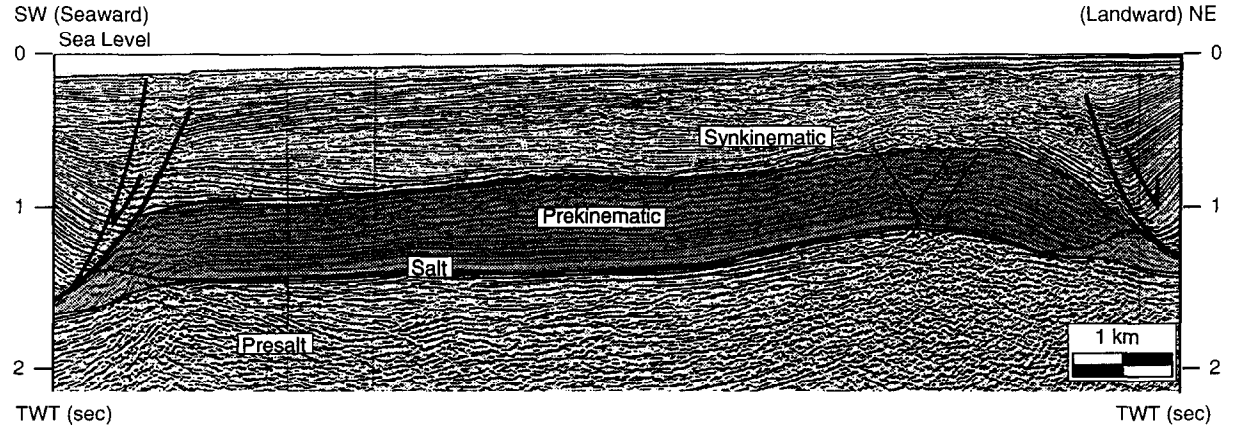

Fig. 8. Seismic image showing an example of a large undeformed raft from the margin.

large undeformed raft below which the ductile layer is homogeneously and strongly sheared. The upper brittle layer is translated without deformation. Figure 8 illustrates a comparable structure in nature. A comparison with the experimental model shows that, for structures where deformation is localized in the basal salt layer, the horizontal displacement can be important. The apparently undeformed aspect in seismic images can therefore lead to a misleading kinematic interpretation.

(3) The upslope deformation domain (Fig. 7c) is characterized by systems of conjugate planar normal faults or even synthetic–antithetic listric normal faults which delimit thick syn-kinematic depocentres. The deformation in the ductile layer is extremely heterogeneous as demonstrated by the contorted passive markers. This is clearly a consequence of complex faulting histories in the overlying brittle layer. On average, the ductile layer is here more vertically thinned than in the two previous deformation domains, thus indicating a higher component of pure shear.

Effects of basal slope angle

Figure 9 illustrates a set of experiments carried out with a 2-cm thick pre-kinematic overburden and a 'low' sedimentation rate (0.4 cm every 2 h). The increase in basal slope leads to a nearly linear increase in the amount of bulk stretching by a factor 3 from 0° to 5°, as well as an increase in the width of the deformed zones.

Low basal slopes angles (0° and 1°) are characterized by a single downslope deformed zone with tilted blocks and associated asymmetric depocentres. Block tilting is controlled by planar or listric synthetic normal faults. Antithetic normal faults are only active during the early stages of deformation. For higher basal slope angles, a second deformation zone develops upslope. Its width (W_u) increases with α together with a correlative decrease in width of the downslope deformation zone (W_d). A central raft, translated without deformation of the overburden, separates the two deformation zones. The total width of the deformation zones ($W_d + W_u$) increases with α leading to a progressive decrease of central raft width. The same type of experiments carried out with a thinner pre-kinematic layer (1 cm) give similar results. Figure 10 presents the evolution of the deformed zone width as a function of basal slope angle. While the total deformed domain width increases with increasing basal slope, this graph displays that the downslope deformed width increases up to 3° at higher slope angles, W_d decreases and W_u increases at the expense of W_d.

Effects of sedimentation rate

In order to explore the potential effects of sedimentation on deformation, two rates of sedimentation were tested, called here for convenience, 'low' (0.2 cm h^{-1}: LSR) and 'high' (0.4 cm h^{-1}: HSR).

Figure 11 shows a comparison of experiments for basal slope angles of 0°, 1° and 2°, with a pre-kinematic overburden of 1 cm. Both types of experiments yield a downslope deformation zone with tilted blocks delimited by synthetic normal faults and/or rafted blocks. As seen in the previous section, and whatever the sedimentation rate, the first structures to develop correspond to symmetric grabens. When sedimentation rate increases the number of rafts or tilted blocks also increases. This effect is enhanced by increasing the basal slope angle. For a 2° basal slope angle, an increase in sedimentation rate leads to a single downslope deformation zone. The comparison between LSR and HSR experiments with a 2° basal slope suggests that an increase in sedimentation rate tends to reinforce downslope deformation and the development of synthetic listric growth faults.

In Fig. 11, LSR and HSR models display similar amounts of bulk stretching, even though the experiment duration is 12 h for LSR models and 6 h for HSR models. This demonstrates that an increase in sedimentation rate enhances the displacement rate.

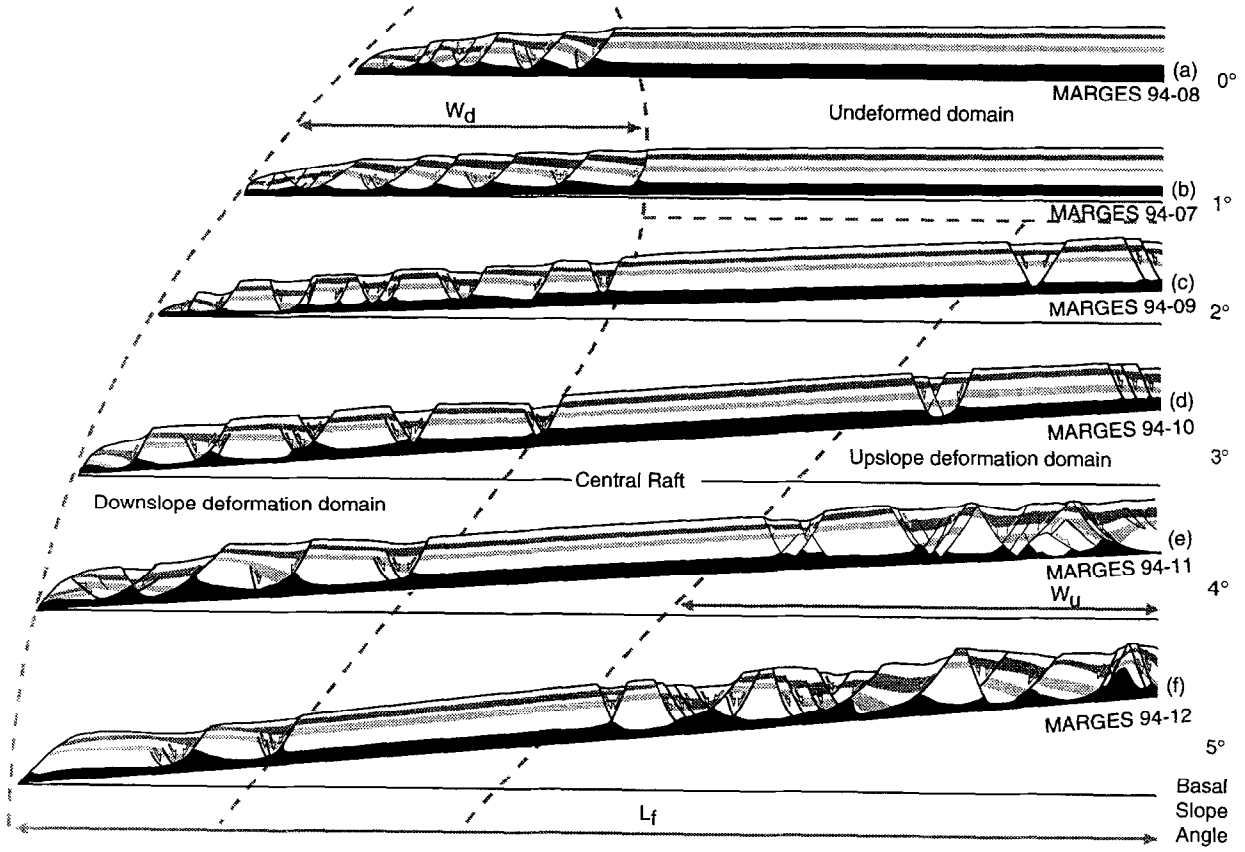

Fig. 9. Domains of overburden deformation in glided slabs as a function of the angle α of basal slope. W_d, width of the downslope deformed domain; W_u, width of the upslope deformed domain; L_f, final length of the slab. See text for explanation.

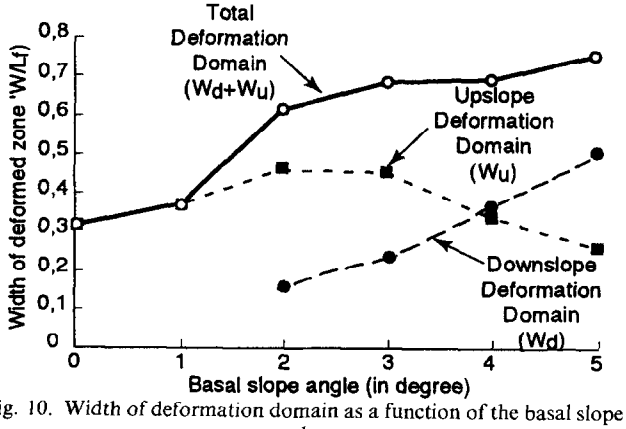

Fig. 10. Width of deformation domain as a function of the basal slope angle α.

CONCLUSIONS AND DISCUSSION

The analysis of natural examples of gravity gliding from the West African margin combined with laboratory-scale modelling leads to the following conclusions concerning the role of basal slope angle and syn-kinematic sedimentation in progressive extension.

(1) *The basal slope angle plays a dominant role on the location of extension.* When the basal layer of potential décollement—the Aptian salt in the case of the West African passive margin—is horizontal or very shallow dipping (0–2°) deformation is concentrated at the front of the margin (Figs 6 & 9). For higher angles of basal slope, three domains of deformation can be distinguished: a downslope (seaward) and an upslope (landward) deformation domain (Figs 7 & 9), where the sedimentary overburden is faulted and delimits local sedimentary depocentres, which are separated by a central domain where the overburden is translated (rafted) without faulting (Figs 7 & 9).

(2) *The width of the extensional domain varies as a function of the basal slope angle.* The width of the downslope deformation domain decreases with increasing α. However, the total width of the deformation increases fairly regularly with α (Fig. 10).

(3) *Early elementary faulting patterns in the sedimentary overburden correspond to symmetric grabens.* During progressive deformation and sedimentation, these grabens can evolve into symmetrical and asymmetrical grabens or tilted blocks. Symmetrical and asymmetrical grabens are characterized by planar or slightly curved normal faults. Tilted blocks result from the localization of displacement on one of the two faults delimiting an early graben, which give rise to a listric normal fault (Figs 6, 7, 9 & 11). In the downslope deformation domains listric normal faults are

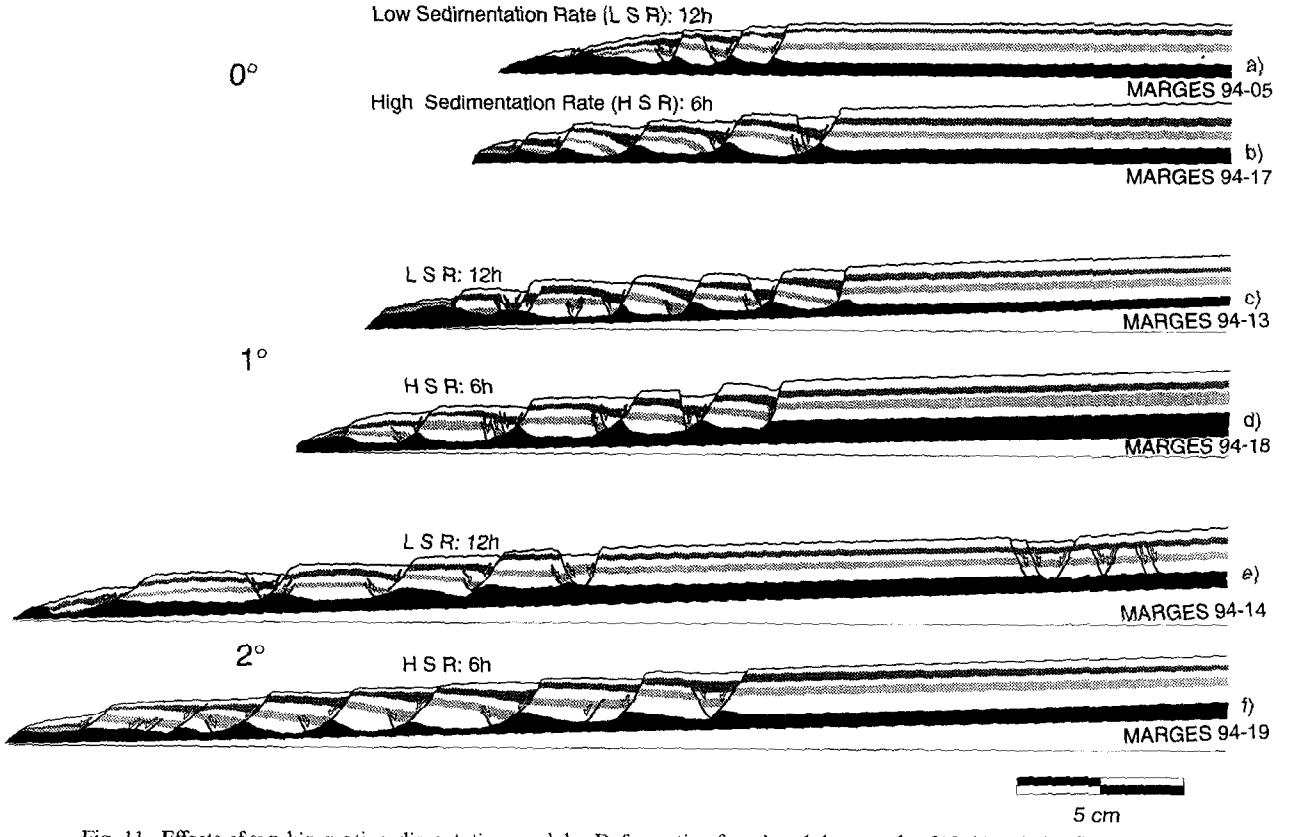

Fig. 11. Effects of syn-kinematic sedimentation on slabs. Deformation for a basal slope angle of 0°, 1° and 2°. LSR and HSR, respectively, for low and high sedimentation rate.

dominantly synthetic. Antithetic normal faults occur quite frequently in the upslope deformation domains (Figs 7, 9 & 11). Occasionally, facing listric normal faults can occur in the upslope deformation domain giving rise to 'turtleback structures'. Figure 12 summarizes the typical structural patterns resulting from the development of early grabens during progressive deformation.

(4) *Deformation of the basal ductile layer results from a combination of pure shear (i.e. layer-perpendicular shortening) and simple shear (i.e. layer-parallel shearing).* This combination varies from point to point along the

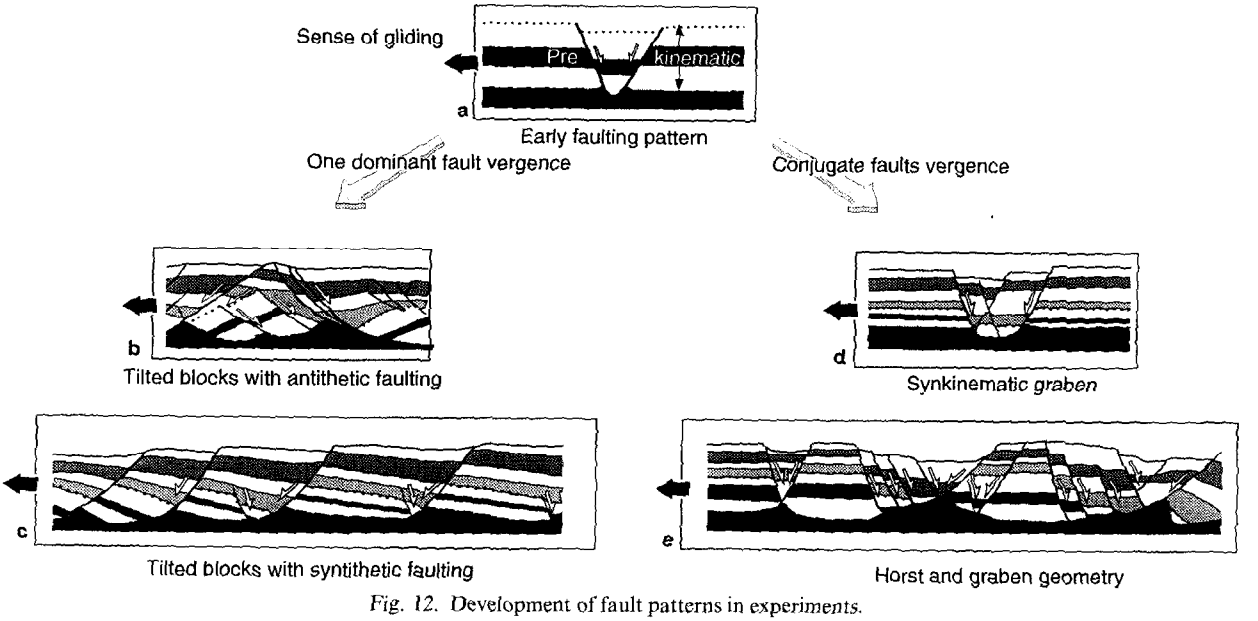

Fig. 12. Development of fault patterns in experiments.

ductile layer. In the upslope deformation domain, the pure-shear component is dominant. Conversely, below the central raft (Fig. 7), flow approached simple shear. Owing to interactions with faulting in the overlying sedimentary layers, finite-strain patterns in the ductile layer become extremely heterogeneous with increasing deformation (Fig. 7). Experiments show, in particular, the complexities of strain patterns occurring below tilted blocks and within salt rollers (Fig. 7).

(5) *Syn-kinematic sedimentation rates exert a control on both displacement rate and extensional patterns.* Increasing sedimentation rates increases the displacement rate and, consequently, the total amount of displacement and bulk stretching of the slided slab. This conclusion is to be expected because the shear stress parallel to the basal décollement is a direct function of the overburden load for a given angle of basal slope. Furthermore, increasing shear stress increases the strain rate in the ductile layer. It is less evident, as demonstrated by experiments, that increasing sedimentation rates enhance and favour the development of synthetic listric normal faults.

The experiments presented in this paper consider only the early development of extensional structures within a slab gliding above a salt layer. In some circumstances compression can occur downslope in the early stages (Cobbold *et al.*, 1989), but more frequently downslope extensional structures are seen to be inverted by late compression (e.g. Demercian *et al.*, 1993; Mohriak *et al.*, 1995; Liro and Coen, 1995; Spathopoulos, 1996). Our results could help in interpretating structures later complicated by inversion.

The conclusions of this paper may have important practical applications in hydrocarbon exploration. The downslope central raft–upslope zonation of deformation gives a reference frame for the reconstruction of sedimentary units and potential prospects. The observed processes of faulting, fault patterns and draping of faults by syn-kinematic sediments are especially interesting in the understanding of hydrocarbon migration and the identification of reservoir distributions and trap geometries. The experiments also show that the upslope deformation domain displays the most extensive syn-kinematic depocentres in comparison to the outermost domains of the slided slabs. Interestingly, these upslope deformation domains are also the most accessible to offshore exploration.

Acknowledgements—This work was financed by Elf Aquitaine Production. Experimental data were acquired during the MARGES project (*Modélisation Analogique des Relations entre la Gravité Et la Sédimentation*, Géosciences Rennes–Elf Aquitaine Production) which aimed to study the interactions between sedimentation and faulting during gravitational deformation. The authors acknowledge Elf for their permission to use seismic data and to publish this paper, and D. Nieuwland and D. Rouby for improving the manuscript. The authors also thank J. J. Kermarrec for invaluable technical assistance during the experiments, and M. Carpenter for improving the English.

REFERENCES

Bally, A. W., Bernouilli, D., Davis, G. A. and Montadert, L. (1981) Listric normal fault. *Oceanologica Acta* **SP**, 87–101.

Brun, J. P. and Merle, O. (1985) Strain patterns in models of spreading–gliding nappes. *Tectonics* **4**, 705–719.

Brun, J. P. and Merle, O. (1988) Experiments on folding in spreading–gliding nappes. *Tectonophysics* **145**, 129–139.

Burollet, P. F. (1975) Tectonique en radeaux en Angola. *Bulletin de la Société géologique de France* **XVII**(4), 503–504.

Byerlee, J. (1968) Brittle–ductile transition in rocks. *Journal of Geophysical Research* **73**, 4741–4750.

Cloos, E. (1968) Experimental analysis of Gulf Coast fracture patterns. *Bulletin of the American Association of Petroleum Geologists* **52**, 420–444.

Cobbold, P., Rossello, E. and Vendeville, B. (1989) Some experiments on interacting sedimentation and deformation above salt horizons. *Bulletin de la Société géologique de France* **3**, 453–460.

Cobbold, P. R. and Szatmari, P. (1991) Radial gravitational gliding on passive margins. *Tectonophysics* **188**, 249–289.

Crans, W., Mandl, G. and Haremboure, J. (1980) On the theory of growth faulting: a geomechanical delta model based on gravity sliding. *Journal of Petroleum Geology* **2**, 265–307.

Davy, P. (1986) *Modélisation Thermo-mécanique de la Collision Continentale*. Mémoires et Documents du CAESS **8**.

Demercian, S., Szatzmari, P. and Cobbold, P. R. (1993) Style and pattern of salt diapirs due to thin-skinned gravitational gliding. Campos and Santos basins, offshore Brazil. *Tectonophysics* **228**, 393–433.

Duval, B., Cramez, C. and Jackson, M. P. A. (1992) Raft tectonics in the Kwanza (Cuenza) basin, Angola. *Marine and Petroleum Geology* **9**, 389–404.

Gaullier, V., Brun, J. P., Guerin, G. and Lecanu, H. (1993) Raft tectonics: the effects of residual topography below a salt décollement. *Tectonophysics* **228**, 363–381.

Hubbert, M.K. (1937) Theory of scales models as applied to the study of geological structures. *Bulletin of the Geological Society of America* **48**, 1459–1520.

Hubbert, M. K. (1951) Mechanical basis for certain familiar geologic structures. *Bulletin of the Geological Society of America* **62**, 355–372.

Jackson, M. P. A. and Cramez, C. (1989) Seismic recognition of salt welds in salt tectonic regimes. In *GCS-SEPM10th Annual Research Conference, Programs and Abstracts, Texas*, pp. 66–89. Society of Economic Paleontologists and Mineralogists, Houston.

Liro, L. M. and Coen, R. (1995) Salt deformation history and postsalt structural trends, offshore southern Gabon, West Africa. In *Salt Tectonics: A Global Perspective*, eds M. P. A. Jackson, D. G. Roberts and S. Snelson, pp. 323–331. American Association of Petroleum Geologists Memoir **65**.

Lundin, E. L. (1992) Thin skin extensional tectonics on a salt detachment, northern Kwanza basin, Angola. *Marina and and Petroleum Geology* **9**, 405–411.

Merle, O. (1986) Patterns of stretch trajectories and strain rates within spreading gliding nappes. *Tectonophysics* **124**, 211–222.

Mohriak, W. U., Macedo, J. M., Castellani, R. T., Rangel, H. D., Barros, A. Z. N., Latgé, M. A., Ricci, J. A., Mizusaki, A. M., Szatmari, P., Demercian, L. S., Rizzo, J. G. and Aires, J. R. (1995) Salt tectonics and structural styles in the deep water province of the Cabo Frio Region, Rio de Janeiro, Brazil. In *Salt Tectonics: A Global Perspective*, eds M. P. A. Jackson, D. G. Roberts and S. Snelson, pp. 305–321. American Association of Petroleum Geologists Memoir **65**.

Nalpas, T. and Brun, J.-P. (1993) Salt flow and diapirism related to extension at crustal scale. *Tectonophysics* **228**, 349–362.

Ramberg, H. (1967) Model of experimentation of the effect of gravity on tectonic processes. *Geophysics* **14**, 307–329.

Spathopoulos, F. (1996) An insight on salt tectonics in the Angola basin, South Atlantic, In *Salt Tectonics*, eds G. I. Alsop, D. J. Blundel and I. Davison, pp. 153–174. Geological Society of London Special Publication **100**.

Szatmari, P., Gruerra, M. C. M. and Pequeno, M. A. (1996) Genesis of large counter regional faults by flow of Cretaceous salt in the South Atlantic Santos Basin, Brazil. In *Salt Tectonics*, eds G. I. Alsop, D. J. Blundell and I. Davison, pp. 259–264. Geological Society of London Special Publication **100**.

Teisserenc, P. and Villemin, J. (1990) Sedimentary basin of Gabon. Geology and oil systems. In *Divergent/Passive Margin Basins*, eds J.

D. Edwards and P. A. Santogrossi, pp. 117–200. American Association of Petroleum Geologists Memoir **48**.

Vendeville, B. (1987) *Champs de Failles et Tectonique en Extension: Modelisation Expérimentale*. Mémoires et Documents du CAESS **15**.

Vendeville, B. and Cobbold, P. R. (1988) How normal faulting and sediments interact to produce listric faults profiles and stratigraphic wedges. *Journal of Structural Geology* **10**, 649–659.

Vendeville, B., Cobbold, P. R., Davy, P., Brun, J.-P. and Choukroune, P. (1987) Physical models of extensional tectonics at various scales. In *Continental Extension Tectonics*, eds M. P. Coward, J. F. Dewey and P. L. Hancock, pp. 95–107. Geological Society of London Special Publication **28**.

Vendeville, B. and Jackson, M. P. A. (1992) The fall of diapirs during thin skinned extension. *Marine and Petroleum Geology* **9**, 354–371.

Vendeville, B. and Jackson, M. P. A. (1992) The rise of diapirs during thin skinned extension. *Marine and Petroleum Geology* **9**, 331–353.